Int. J. Heat Mass Transfer. Vol. 24, No. 7, pp. 1257–1266, 1981
Printed in Great Britain

0017–9310/81/071257–10 $02.00/0
Pergamon Press Ltd.

CRITICAL HEAT FLUX AND DROPLET ENTRAINMENT RATE IN BOILING OF FALLING LIQUID FILMS

TATSUHIRO UEDA, MITSURU INOUE and SEICHI NAGATOME
Department of Mechanical Engineering, University of Tokyo, Bunkyo-ku, Tokyo, Japan

(*Received* 8 *August* 1980)

Abstract—Measurements of critical heat flux and rate of droplet entrainment due to bubble bursting are made with boiling liquid films flowing downwards on the outside surface of a uniformly heated vertical tube. The critical condition occurs first at the exit end of the heating section. The critical heat flux shows three types of characteristics by increasing the liquid film flow rate at the exit end of the heating section. The data are expressed in terms of the film flow rate and the film Weber number at the exit end. The relationship between the droplet entrainment rate and the evaporation rate of the film is also discussed.

NOMENCLATURE

D,	diameter of heating section;
D_{EB},	entrained droplet flow rate;
g,	acceleration of gravity;
h,	heat transfer coefficient;
h_{fg},	heat of vaporization;
L,	length of heating section;
L_s,	boiling length;
M_f,	liquid film flow rate;
m_{EB},	droplet entrainment rate;
q,	heat flux;
Re,	film Reynolds number, $Re = 4\Gamma/\mu_l$;
u,	liquid velocity;
u_m,	mean velocity of liquid film;
y,	distance from wall surface;
y_i,	film thickness;
y_{im},	film thickness at a mean flow rate.

Greek symbols

Γ,	liquid film flow rate per unit periphery;
μ_l,	liquid viscosity, $\mu_l = \rho_l \nu_l$;
ρ_g,	vapor density;
ρ_l,	liquid density;
σ,	surface tension;
τ_w,	wall shear stress;
ϕ, ϕ',	contact angle, superficial contact angle.

Subscripts

c,	critical heat flux condition;
ex,	exit end of heating section;
in,	inlet end of heating section.

1. INTRODUCTION

BOILING heat transfer to liquid films and film breakdown associated with increasing heat flux have been studied [1, 2] in connection with thin film evaporators and cooling systems of high temperature surfaces, and also studied [3, 4] with a view to obtaining an understanding of the critical heat flux phenomenon which is especially important in high performance flow boiling systems. In a system of a liquid film flowing on a heated surface, the film flow rate decreases as the film flows down along the surface by evaporation and droplet entrainment due to bubble bursting through the film. When the heat flux is increased under such conditions, the liquid film flow rate at the exit end of the heating section decreases progressively, and a point—the so-called critical heat flux condition—is reached where a sharp rise in surface temperature begins near the exit end of the heating section.

In this study, measurements were made of the critical heat flux and the droplet entrainment rate with falling liquid films flowing downwards on the outside surface of a uniformly heated vertical tube. The test liquids used in this study were water, fluorocarbon R-113 and R-11 at near atmospheric pressure. When the film flow rate at the exit end of the heating section was reduced to some value near zero, the sharp rise in wall temperature took place due to formation of stable dry patches in the thin film at the exit end. Fujita and Ueda [4] investigated this case with saturated water films. However, in case of high film flow rates and high heat fluxes, a sharp rise in wall temperature even occurred when a considerable amount of liquid existed at the exit end of the heating section. Therefore, the relation between the critical heat flux and the exit film flow rate was examined.

It has been noted that droplets are formed when vapor bubbles burst on the vapor–liquid interface [5, 6], however, experimental data are limited on the droplet entrainment from boiling liquid films. The droplet entrainment rate seems to be related closely to the boiling situation on the heated surface. In this paper, the relation between the droplet entrainment rate and the evaporation rate is discussed based on the data obtained.

2. APPARATUS AND PROCEDURE

A schematic diagram of the apparatus is shown in Fig. 1. The test section was composed of an intake region made of copper rod, a heating section and a copper tube. The tube was silver-soldered to the lower end of the heating section, and arranged vertically in a

HMT 24:7 - L

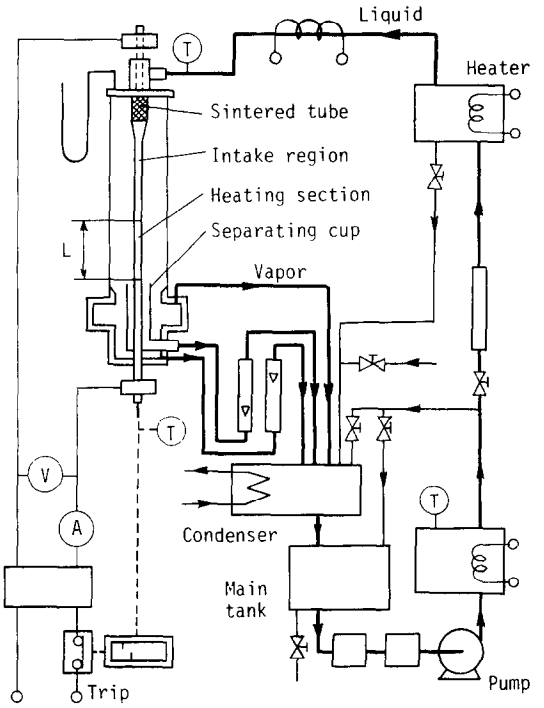

FIG. 1. Schematic diagram of experimental apparatus.

glass tube of 96 mm I.D. The length of the intake region was 400 mm. The heating section, a stainless-steel tube of 8.0 mm O.D. and 180 mm long, was heated uniformly by passing an alternating current through it.

The liquid heated near the saturation temperature, the degree of subcooling being about 4°C, passed through a porous sintered tube and flowed, as a film, down the outside surface of the intake region and the heating section. Most of the droplets dispersed from the film deposited on the outer glass tube and flowed down along the surface. The liquid film flowed down the exit end of the heating section was separated from the droplets with a separating cup of 22 mm I.D. near the exit end of the heating section. The vapor generated from the heating section was led downwards in the glass tube and exhausted to a condenser.

To measure the wall temperature of the heating section, three thermocouples were fitted to the inner surface at distances of 30, 130 and 170 mm from the upper end of the heating section. The outer surface temperature was evaluated taking into account the temperature drop through the tube wall. The sharp rise in wall temperature was detected by the thermocouple located at 170 mm (10 mm above the exit end of the heating section).

The liquid film flow rate at the exit end of the heating section decreased with increasing power input to the heating section. Under the condition of the inlet flow rate kept at a given value, the power input was increased step-by-step at small increments until the sharp rise in wall temperature took place. At each power level, measurements were made of the wall temperature and the film flow rate at the exit end. The critical heat flux was determined as a heat flux just before the sharp rise in wall temperature. As for the R-113 films, measurements were also performed by reducing the inlet liquid flow rate under a constant heat flux. Experimental ranges of the inlet film Reynolds number Re_{in} and the heat flux q were as follows: $Re_{in} = 1400 \sim 13\,400$ and $q \sim 1.1 \times 10^6$ W m^{-2} for water; $Re_{in} = 500 \sim 15\,100$ and $q \sim 0.8 \times 10^5$ W m^{-2} for fluorocarbon R-113, and $Re_{in} = 1100 \sim 14\,400$ and $q \sim 1.1 \times 10^5$ W m^{-2} for R-11.

3. BOILING HEAT TRANSFER

Heat transfer to the film flow in the developed nucleate boiling region was measured at a location 130 mm downstream from the upper inlet end of the heating section. Figure 2 shows the results obtained at atmospheric pressure, where the heat transfer coefficient h is plotted against the heat flux q. The value h is in proportion to four-fifths the power of q and insensitive to the film flow rate.

Nishikawa and Fujita [7–9] proposed correlations of the nucleate boiling heat transfer for pool boiling systems. The dotted lines for water in Fig. 2, which were derived from the correlation for a high heat flux range, represent the relations for the characteristics length of the heating surface R being 0.04, 0.02 and 0.01 m, respectively. The dotted lines for R-113 and R-11 show the experimental results obtained by Nishikawa, Fujita and Hidaka [10] for pool boiling of a high heat flux range with a horizontal upward heating surface of $R = 0.02$ m. The nucleate boiling heat transfer coefficient for falling films is then regarded as to be similar to that for pool boiling.

4. CRITICAL HEAT FLUX IN FALLING LIQUID FILMS

4.1. *Experimental results*

Figure 3 shows the critical heat flux plotted against the liquid film flow rate at the inlet of the heating section

$$\Gamma_{in} = M_{fin}/\pi D.$$

The critical heat flux increases with increasing inlet film flow rate: steeply for a range of low flow rates and gently for high flow rates. The dotted lines indicate, for reference, the values

$$q = \Gamma_{in} h_{fg}/L$$

required for complete evaporation of the liquid film.

The sharp rise in wall temperature took place always at the exit end of the heating section. It will be, therefore, needed to consider the relation between the critical heat flux and the exit film flow rate

$$\Gamma_{ex} = M_{fex}/\pi D.$$

Figure 4 shows the relationships. As is seen in this figure, characteristics of the critical heat flux can be divided into three types in order of increasing the exit film flow rate.

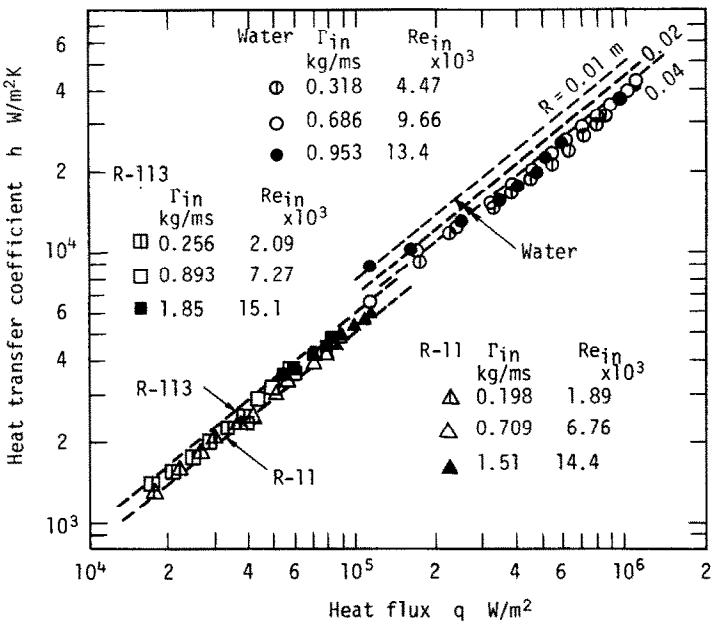

FIG. 2. Heat transfer coefficient in nucleate boiling region.

The critical condition of the type I was mainly observed in the experiment made by Fujita and Ueda [4] with long heating sections. There, the exit film flow rate decreased with increasing heat flux, in a state of relatively uniform film around the tube periphery, to a very low value in a range of $\Gamma_{ex} = 0.01$–$0.02\,\mathrm{kg\,m^{-1}\,s^{-1}}$, and then the critical condition took place by forming a large permanent dry patch at the exit end of the heating section. Therefore, it can be considered that the critical condition of type I occurs when the exit film flow becomes less than the minimum wetting rate, i.e. the minimum liquid flow rate required to wet the surface after formation of a dry patch. In the situation of the minimum wetting rate, the dynamic force of the thin film balances with the surface tension at the upper end of the dry patch, as shown in Fig. 5. In practice, the dynamic force is fluctuating with time by wave motion on the film. Then, the force balance for the dry patch being permanent will be given by

$$\left[\frac{1}{2}\int_0^{y_i}\rho_l u^2\,\mathrm{d}y\right]_{\max} = \sigma(1-\cos\phi) \qquad (1)$$

where ϕ is the contact angle. Therefore, once the film of flow rate less than the minimum wetting rate is disrupted, the liquid can no longer re-wet the surface and the wall temperature can rise sharply regardless of the heat flux level.

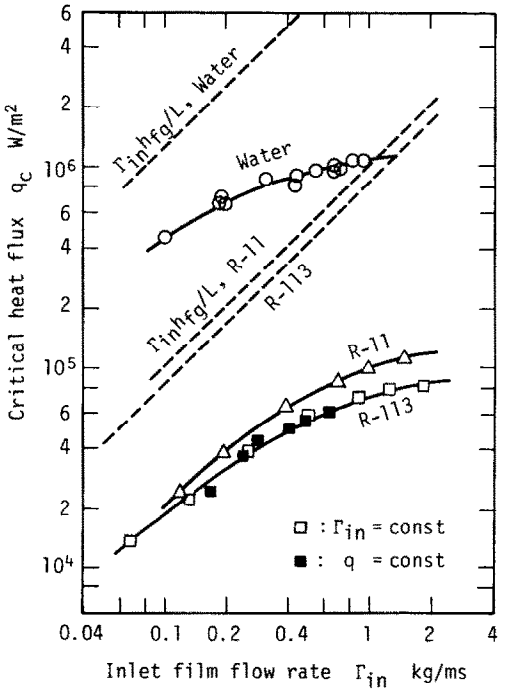

FIG. 3. Critical heat flux and inlet film flow rate.

The critical phenomena of types II and III were observed in the present experiment. In the region of type II where the critical heat flux increases with increasing the exit film flow rate, the liquid film involving vapor bubbles was distorted around the tube periphery as the heat flux increased [Fig. 6(a)], and a large stable dry patch giving rise to the sharp rise in wall temperature was formed in a thinned film area. In the region of type III, on the other hand, there was a considerable amount of liquid flowing at the exit end. The film flowed down covering the tube periphery almost entirely. When the heat flux was increased near the critical value, the main part of the film on the exit end of the heating section appeared to be separated from the heating surface. In this condition, the heating surface, observed occasionally through disrupted portions of the main film, was covered with a thin liquid film with nucleate boiling, as is seen in Fig. 6(b-2). This state of the thin film was maintained until the heat flux

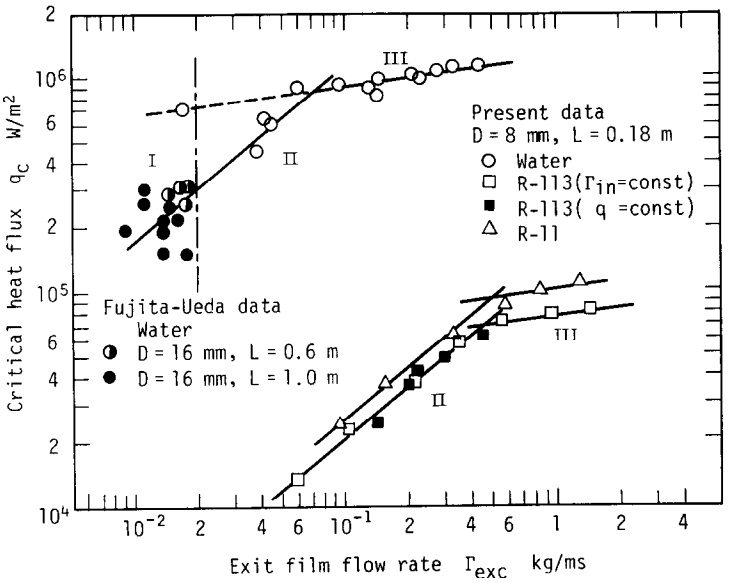

FIG. 4. Relation between critical heat flux and exit film flow rate.

was raised to the critical value, however, when the heat flux increased over the critical value, the sharp rise in wall temperature occurred accompanied with local boiling up of the thin film.

The thin film left on the surface has fairly high cooling capacity, but its capacity decreases with decreasing its flow rate by evaporation. Therefore, it is difficult to specify the liquid film flow state at the critical heat flux condition of type III. However, it may be possible to consider that an essential phenomenon in the process to reach the critical condition of type III is the main film separation, although the film separation starts at a heat flux lower than the critical value.

4.2. *Discussion and correlation*

For discussing the liquid film flow rate at critical condition, it is useful to introduce the mean velocity and thickness of the liquid film. The film flow rate per unit periphery

$$\Gamma = \rho_l u_m y_i \tag{2}$$

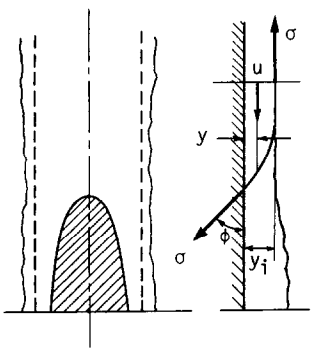

FIG. 5. Steady dry patch.

is expressed as

$$\Gamma = \rho_l \int_0^{y_i} u\,dy = \mu_l \int_0^{y_i^+} u^+\,dy^+ \tag{3}$$

where

$$u^+ = u\Big/\left(\frac{\tau_w}{\rho_l}\right)^{0.5}, \quad y^+ = \frac{y}{\nu_l}\left(\frac{\tau_w}{\rho_l}\right)^{0.5}.$$

If it is assumed that no vapor bubble is involved in the film and the velocity distribution in the film can be approximated by the universal velocity profile, the following well-known results are obtained

$$\left.\begin{aligned} \Gamma/\mu_l &= (y_i^+)^2/2 && y_i^+ < 5 \\ \Gamma/\mu_l &= 12.5 - 8.05\,y_i^+ + 5y_i^+ \ln y_i^+ && 5 \leqq y_i^+ < 30 \\ \Gamma/\mu_l &= -64 + 3y_i^+ + 2.5y_i^+ \ln y_i^+ && y_i^+ \geqq 30. \end{aligned}\right\} \tag{4}$$

Therefore, the non-dimensional film thickness

$$y_i^+ = \frac{y_i}{\nu_l}\left(\frac{\tau_w}{\rho_l}\right)^{0.5} \tag{5}$$

is found from the measured film flow rate. For the falling liquid films, the wall shear stress is given by

$$\tau_w = \rho_l g y_i. \tag{6}$$

Then, the thickness and mean velocity of the liquid film can be obtained by the following equations

$$y_i = \left[\frac{(\nu_l y_i^+)^2}{g}\right]^{1/3}, \quad u_m = \frac{\Gamma}{\rho_l y_i}. \tag{7}$$

An attempt was made to correlate the critical heat flux to the film thickness y_{ic} and the mean film velocity u_{mc} thus derived for the measured exit film flow rate at the critical condition Γ_{exc}.

4.2.1. *Region of type I.* As mentioned before, the boundary of the region I seems to be connected with

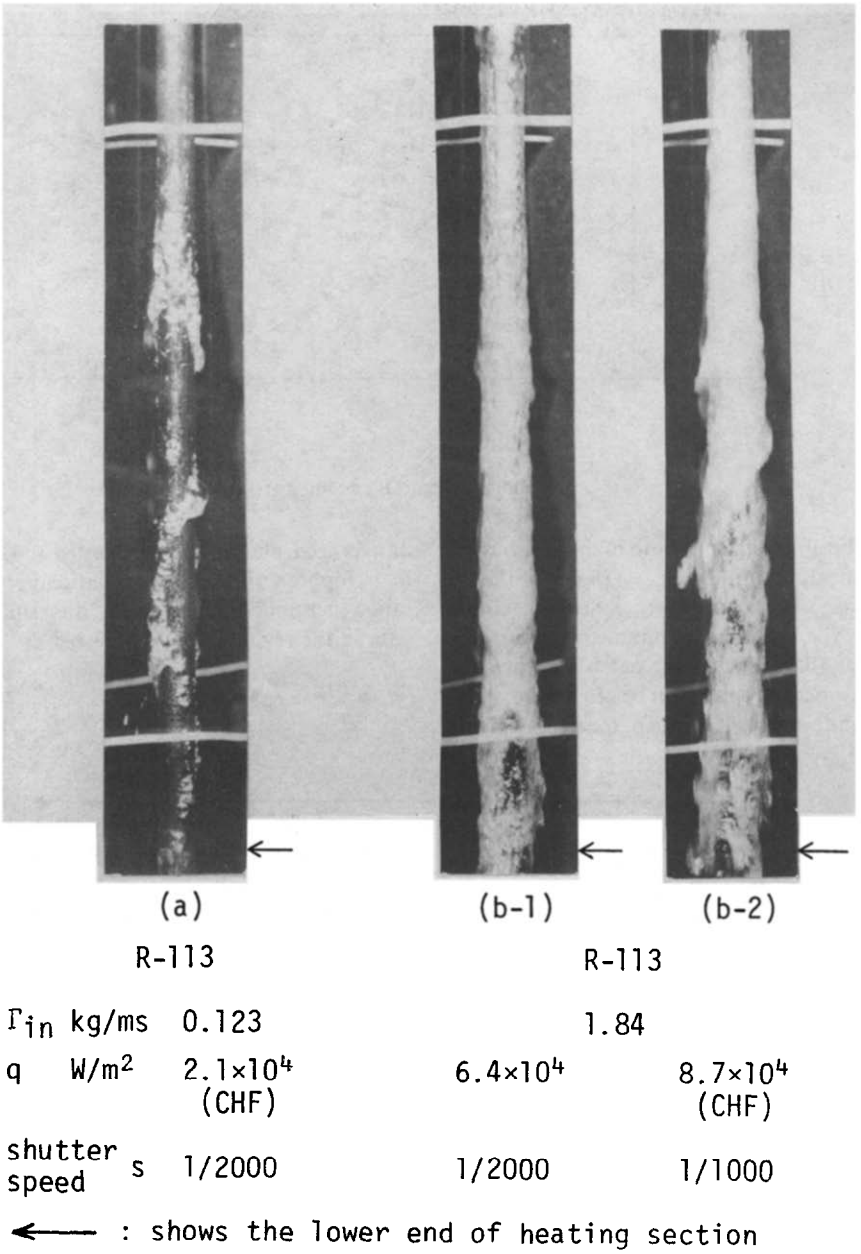

FIG. 6. Liquid film flow in regions II and III.

the minimum wetting rate for falling films. Norman and McIntyre [11] measured the minimum wetting rate and found to be about $\Gamma = 0.01\ \mathrm{kg\ m^{-1}\ s^{-1}}$ for isothermal water films. However, it is noted that this rate is affected by many factors [12, 13]. Therefore, it is difficult to predict the upper limit of the region I definitely, but the limiting value is estimated from Fig. 4 to be about $0.02\ \mathrm{kg\ m^{-1}\ s^{-1}}$ for water films. This condition of $\Gamma_{exc} = 0.02\ \mathrm{kg\ m^{-1}\ s^{-1}}$ for saturated water films can be expressed by applying the mean velocity and film thickness as follows:

$$\rho_l u_{mc}^2 y_{ic}/\sigma = 0.06. \quad (8)$$

This equation may be used tentatively as a boundary of the region I. This boundary is corresponding to put the superficial contact angle $\phi' = 15°$ in the following expression

$$\rho_l u_{mc}^2 y_{ic}/2 = \sigma(1-\cos\phi').$$

4.2.2. *Region of type II.* In this region, the dynamic force of the film averaged around the tube periphery is in the relation of

$$\rho_l u_{mc}^2 y_{ic}/2 > \sigma(1-\cos\phi').$$

However, when the evaporation rate of the film, $q/h_{fg} = \rho_g u_g$, was increased, the boiling film distortion and local thinning of the film were observed. The sharp rise in wall temperature took place usually by forming a large dry patch in a thinned film area. The boiling film distortion appeared to be caused by non-uniformity of nucleation sites on the heated surface.

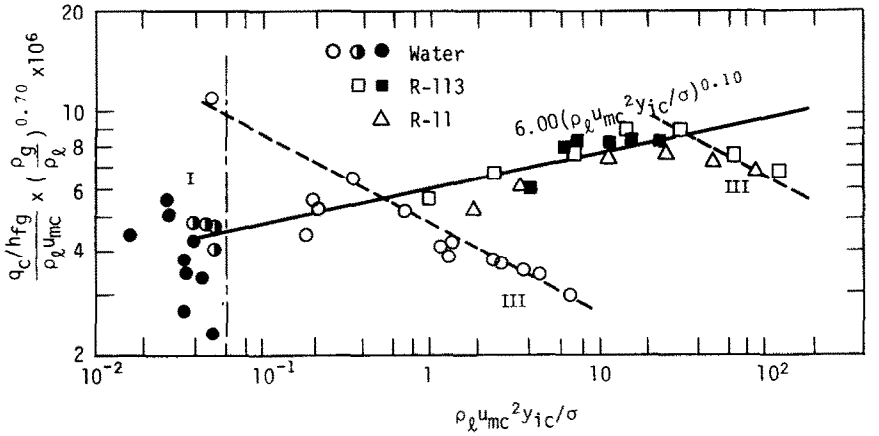

FIG. 7. Correlation of critical condition (type II).

Based on the observation, a ratio of the evaporation rate at the critical condition, $q_c/h_{fg} = (\rho_g u_g)_c$, to the exit flow rate, $\rho_l u_{mc}$, was considered. Since the critical condition of type II occurs by film disruption due to appearance of a large stable dry patch in a distorted film, a high evaporation rate will be required to reach the critical condition when a ratio of the dynamic force of averaged film to the surface tension, $\rho_l u_{mc}^2 y_{ic}/\sigma$, is high. Figure 7 shows the correlation between the two ratios mentioned above. Then, the critical condition data in the region II was expressed as

$$\frac{q_c/h_{fg}}{\rho_l u_{mc}} = 6.00 \times 10^{-6} \left(\frac{\rho_g}{\rho_l}\right)^{-0.70} \left(\frac{\rho_l u_{mc}^2 y_{ic}}{\sigma}\right)^{0.10}. \quad (9)$$

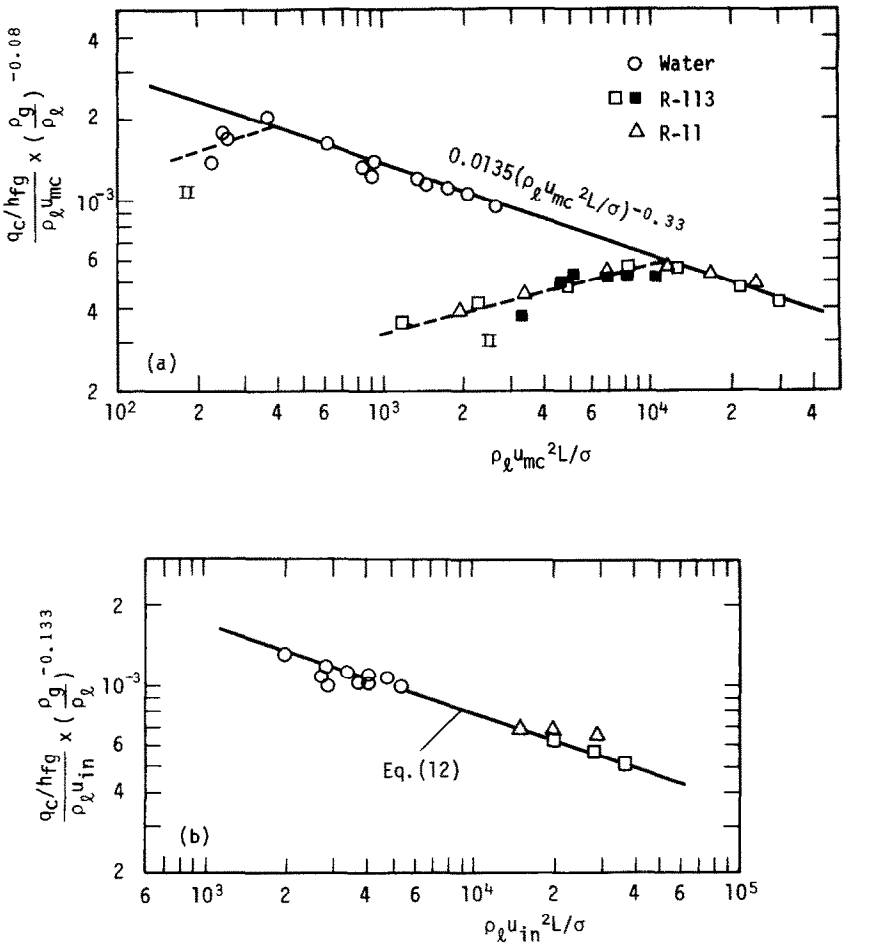

FIG. 8.(a) Correlation of critical condition (type III). (b) Comparison with equation (12).

The dotted lines in Fig. 7 are those for the data in the region III. A point showing the highest heat flux in the region I was obtained accidentally with a less distorted film. It is interesting to note the point is on an extension of the dotted line for water films.

4.2.3. *Region of type III.* Kutateladze and Leontév [14] considered a stream of density ρ_0 and velocity U_0 flowing on a permeable flat plate with fluid injection, and gave the critical injection rate for boundary layer separation from the plate as follows:

$$(\rho_{in}U_{in})_c = 2f\rho_0 U_0 \tag{10}$$

where, ρ_{in} and U_{in} are the density and velocity of the injected fluid, and f is the friction factor for the main stream without fluid injection. On the basis of this concept, Tong [15] presented a semi-empirical correlation for the critical heat flux condition in the following form

$$\frac{q_c/h_{fg}}{\rho_l U_0} = f(x)\, Re_l^{-0.6} \tag{11}$$

where U_0 is the main stream velocity, $f(x)$ is a function of the bulk quality and Re_l is the liquid Reynolds number.

Equation (11) is the one proposed for the critical condition in subcooled and low-quality regions, and is not for that of film flow boiling. However, such a method to express the ratio of the evaporation rate to the liquid flow rate in terms of some flow parameters as equation (11) seems to be useful to correlate the critical heat flux in film flow boiling with main film separation. Katto and Ishii [16] measured the critical heat flux with a saturated liquid jet flowing over high heat flux surfaces of $L = 0.01 \sim 0.02$ m, and showed the critical condition data were well correlated, irrespective of the liquid jet thickness, by the following equation

$$\frac{q_c/h_{fg}}{\rho_l u_e} = 0.0164\left(\frac{\rho_g}{\rho_l}\right)^{0.133}\left(\frac{\rho_l u_e^2 L}{\sigma}\right)^{-0.33} \tag{12}$$

where u_e denotes the velocity of the liquid jet.

Taking into account the results mentioned above, the present data in the region III were plotted on the coordinates shown in Fig. 8(a). The abscissa represents the Weber number of the exit film flow defined for the heating length

$$We = \rho_l u_{mc}^2 L/\sigma.$$

The critical heat flux is supposed to depend mostly on the local flow parameters at the exit end of the heating section. In the correlation of Fig. 8(a), the exit film velocity u_{mc} is used, however, this value is the one derived by neglecting the vapor bubbles in the film. The liquid film in the region of type III involves many bubbles in it. The bubble density or void fraction in the film will have an important effect on the critical condition and also on the film separation. Visual studies of the film flow showed a clear trend of the bubble density to increase along the heating length. This trend is suggesting that the heating length has an effect not only on the exit film flow state but on the critical heat flux. By this reasoning, the Weber number defined for the heating length is introduced to correlate the critical condition of the type III.

As is seen in Fig. 8(a), the critical condition data in the region III can be expressed as

$$\frac{q_c/h_{fg}}{\rho_l u_{mc}} = 0.0135\left(\frac{\rho_g}{\rho_l}\right)^{0.08}\left(\frac{\rho_l u_{mc}^2 L}{\sigma}\right)^{-0.33}. \tag{13}$$

This equation is similar to equation (12) of Katto and Ishii, however, somewhat different in its definition. The liquid velocity u_e in equation (12) denotes the value at the inlet of the heating section. For comparing with equation (12), the present data of type III were also plotted on the coordinates of $(q_c/h_{fg})/\rho_l u_{in}$ and $\rho_l u_{in}^2 L/\sigma$, as shown in Fig. 8(b). Here, u_{in} represents the mean film velocity derived by equations (4)–(7) for the inlet film flow rate Γ_{in}. The present data agree well with equation (12) in spite of a great difference in heating length used in the tests. This fact along with the visual observation of the film flow state suggests, as well as the case of Katto and Ishii, that the critical condition of the type III is closely connected with the main film separation resulting from high vapor generation on the heated surface.

The boundary of the regions II and III can be expressed as the intersection of equations (9) and (13) as follows:

$$\left(\frac{\rho_g}{\rho_l}\right)^{0.78}\left(\frac{\rho_l u_{mc}^2}{\sigma}\right)^{-0.43} \Big/ (y_{ic}^{0.10} L^{0.33}) = 4.44 \times 10^{-4}. \tag{14}$$

5. DROPLET ENTRAINMENT RATE

The droplet flow rate dispersed by boiling was calculated from the following equation by applying the film flow rates Γ_{in} and Γ_{ex} measured at the inlet and exit of the heating section and the heat flux q

$$D_{EB} = \pi D(\Gamma_{in} - \Gamma_{ex}) - \pi D L_s q/h_{fg} \tag{15}$$

and the droplet entrainment rate per unit surface area was derived by

$$m_{EB} = D_{EB}/(\pi D L_s) \tag{16}$$

where L_s is the tube length from the location where the bulk temperature of the film reaches the saturation value to the exit end of the heating section. Since the temperature of the liquid supplied to the test section was a little lower than the saturation temperature, there was a subcooled region in the heating length. The length of the subcooled region was short and we could approximate as $L \approx L_s$ in case of high heat fluxes near the critical condition, however, the length was not so short in case of low heat fluxes. Then, the boiling length L_s was used for determining the droplet entrainment rate. For measuring the exit film flow rate, three different separating cups of 18, 22 and 26 mm I.D. were tested. The difference among these measured values was generally small, then, the data obtained with a cup of 22 mm I.D. were used for this calculation.

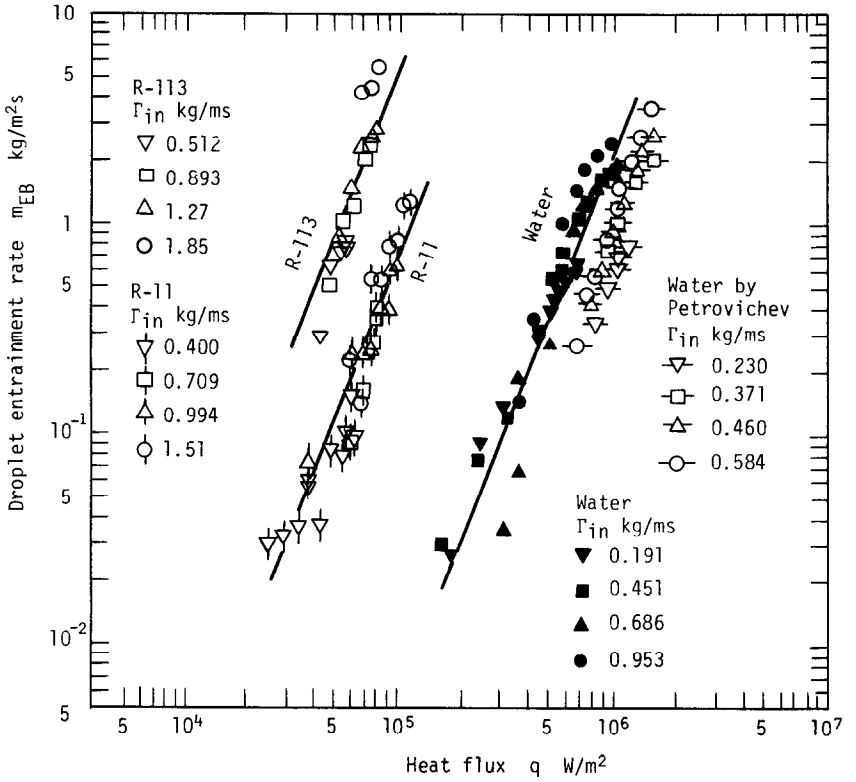

FIG. 9. Droplet entrainment rate.

Figure 9 shows data of the droplet entrainment rate thus derived. The droplet entrainment rate is in proportion to the 2.5 power of heat flux, and shows a trend to increase with increasing liquid film flow rate Γ_{in}. The data of Petrovichev *et al.* [17] are plotted in this figure for reference, which were obtained for water films with a stainless-steel heating section of 9 mm O.D. and 50 mm long.

The data shown in Fig. 9 are separated widely according to properties of the liquid film. Comparison of these three curves suggests that the droplet rate is affected by the superficial vapor velocity u_g as well as the evaporation rate, $\rho_g u_g = q/h_{fg}$. Then, an attempt was made to correlate the ratio of the droplet rate to the evaporation rate, $m_{EB}/(q/h_{fg})$, to the vapor Weber number

$$\frac{\rho_g u_g^2 y_{im}}{\sigma} = \frac{(q/h_{fg})^2 y_{im}}{\sigma \rho_g} \tag{17}$$

where y_{im} denotes the film thickness obtained by equations (4)–(7) for the mean film flow rate, $\Gamma_m = (\Gamma_{in} + \Gamma_{ex})/2$. Figure 10 shows the results in which the data are correlated by the following equation

$$\frac{m_{EB}}{q/h_{fg}} = C\left[\frac{(q/h_{fg})^2 y_{im}}{\sigma \rho_g}\right]^{0.75} \tag{18}$$

where C is a constant, $C = 4.77 \times 10^2$ for water, $C = 6.63 \times 10^2$ for R-113 and $C = 1.33 \times 10^2$ for R-11. The reason is not clear why the value C is dependent on the liquid, however, as in case of nucleate boiling heat transfer [18], it seems to be related to such factors as the nucleation site density described by the liquid–surface combination.

6. CONCLUSIONS

From the experimental data and discussion on the critical heat flux and the droplet entrainment rate in boiling of falling liquid films, the following conclusions are obtained:

(1) The critical heat flux condition occurred at the exit end of the heating section can be divided into three types according to the exit film flow rate.

Type I: The critical condition is caused by a reduction of the exit film flow rate to an extremely low value near zero, irrespective of the heat flux added.

Type II: The boiling film is distorted and the critical condition takes place by forming a stable dry patch in a thinned film area near the exit end.

Type III: The critical condition seems to be associated with main film separation resulting from high vapor generation on the heated surface.

(2) For correlating the critical condition data, equations (9) and (13) are derived experimentally for the regions of type II and type III, respectively.

(3) Droplet entrainment rate in liquid film boiling depends strongly on the evaporation rate and shows a trend to increase with increasing film thickness. The data are correlated in a form of equation (18).

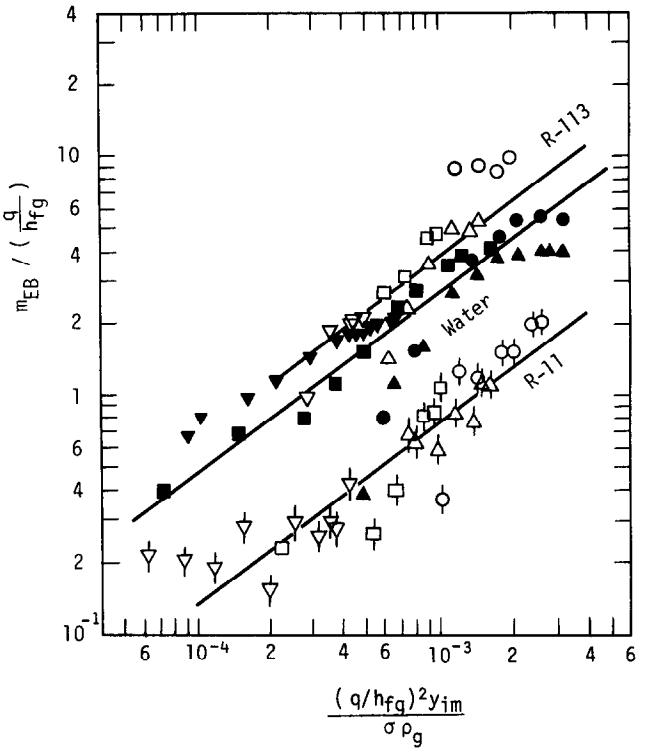

FIG. 10. Correlation of droplet entrainment rate. The key is given in Fig. 9.

Acknowledgements—The authors would like to thank Mr M. Tawra for his cooperation. This work was supported by the research fund (Grant in Aid of Scientific Research, 1976 and 1978) of the Ministry of Education, Japan.

REFERENCES

1. G. F. Hewitt and N. S. Hall-Taylor, *Annular Two-Phase Flow*, Chap. 7, pp. 127–135. Pergamon Press, Oxford (1970).
2. G. L. Shires, A. R. Pickering and P. T. Blacker, Film cooling of vertical fuel rods, AEEW-R343 (1964).
3. G. F. Hewitt, H. A. Kearsey, P. M. C. Lacey and D. J. Pulling, Burnout and nucleation in climbing film flow, *Int. J. Heat Mass Transfer* **8**, 793–814 (1965).
4. T. Fujita and T. Ueda, Heat transfer to falling liquid films and film breakdown—II. Saturated liquid films with nucleate boiling, *Int. J. Heat Mass Transfer* **21**, 109–118 (1978).
5. F. H. Garner, S. R. M. Ellis and J. A. Lacey, The size distribution and entrainment of droplets, *Trans. Inst. chem. Engrs* **32**, 222–235 (1954).
6. D. N. Newitt, N. Dombrowski and F. H. Knelman, The mechanism of drop formation from gas or vapour bubbles. *Trans. Instn chem. Engrs* **32**, 244–260 (1954).
7. K. Nishikawa, Y. Fujita and T. Matsuo, On the correlation of nucleate boiling heat transfer based on the bubble population, *Trans. Jap. Soc. Mech. Engrs* **41-347**, 2141–2150 (1975).
8. K. Nishikawa and Y. Fujita, On the nucleation factor in nucleate boiling heat transfer, *Trans. Jap. Soc. Mech. Engrs* **41–347**, 2151–2159 (1975).
9. Y. Fujita and K. Nishikawa, On the pressure correlation term in the correlating equation of nucleate boiling heat transfer, *Trans. Jap. Soc. Mech. Engrs* **42–361**, 2871–2878 (1976).
10. K. Nishikawa, Y. Fujita and S. Hisaka, Nucleate boiling heat transfer to fluorocarbon refrigerants, *Proc. 14th Japan National Heat Transfer Symp.*, pp. 130–132 (1977).
11. W. S. Norman and V. McIntyre, Heat transfer to a liquid film on a vertical surface, *Trans. Instn chem. Engrs* **38**, 301–307 (1960).
12. V. A. Hallett, Surface phenomena causing breakdown of falling liquid films during heat transfer, *Int. J. Heat Mass Transfer* **9**, 283–294 (1966).
13. T. Fujita and T. Ueda, Heat transfer to falling liquid films and film breakdown—I. Subcooled liquid films, *Int. J. Heat Mass Transfer* **21**, 97–108 (1978).
14. S. S. Kutateladze and A. I. Leontév. Some applications of the asymptotic theory of the turbulent boundary layer. *Proc. 3rd Int. Heat Transfer Conf.* **5**, 1–6 (1966).
15. L. S. Tong, Boundary-layer analysis of the flow boiling crisis, *Int. J. Heat Mass Transfer* **11**, 1208–1211 (1968).
16. Y. Katto and K. Ishii, Burnout in a high heat flux boiling system with a forced supply of liquid through a plane jet, *Proc. 6th Int. Heat Transfer Conf.* **1**, 435–440 (1978).
17. V. I. Petrovichev, L. S. Kokorev, A. Ya. Didenko and G. P. Dubvrovskiy, Droplet entrainment in boiling liquid films, *Heat Transfer—Soviet Research* **3–1**, 19–22 (1971).
18. W. M. Rohsenow, A method of correlating heat transfer data for surface boiling of liquids, *Trans. ASME* **74**, 969–976 (1952).

FLUX DE CHALEUR CRITIQUE ET TAUX D'ENTRAINEMENT DES GOUTTELETTES DANS DES FILMS LIQUIDES EN EBULLITION

Résumé—Des mesures de flux de chaleur critiques et de taux d'entraînement de gouttelettes dûs à l'éclatement de bulles sont effectuées sur des films liquides en ébullition qui descendent le long de la surface externe d'un tube vertical uniformément chauffé. La condition critique s'obtient en premier à l'extrémité de sortie de la section de chauffage. Ce flux de chaleur critique correspond à trois types de caractéristiques de façon à augmenter le débit du film liquide à l'extrémité de sortie, et les données sont exprimées en fonction du débit du film et du nombre de Weber du film à la section de sortie. On discute aussi la formule entre le taux d'entraînement de gouttelettes et le taux d'évaporation du film.

KRITISCHE WÄRMESTROMDICHTE UND TROPFENBELADUNG BEIM SIEDEN VON RIESELFILMEN

Zussammenfassung—An siedenden Rieselfilmen auf der Außenseite gleichförmig beheizter vertikaler Rohre wurden Messungen der kritischen Wärmestromdichte und der Tropfenbeladung durch das Aufplatzen von Blasen durchgeführt. Die kritische Bedingung tritt zuerst am Ende der Heizstrecke auf. Die kritische Wärmestromdichte zeigt bei Vergrößerung des Filmmassenstroms am Ende der Heizstrecke drei charakteristische Erscheinungsformen; die Versuchswerte werden mittels des Filmmassenstroms und der Film-Weber-Zahl am Austritt dargestellt. Weiter wird die Beziehung zwischen der Tropfenbeladung und der Verdampfungsgeschwindigkeit des Films behandelt.

КРИТИЧЕСКИЙ ТЕПЛОВОЙ ПОТОК И СКОРОСТЬ УНОСА КАПЕЛЬ ПРИ КИПЕНИИ СТЕКАЮЩИХ ПЛЕНОК ЖИДКОСТИ

Аннотация — Проведены измерения величины критического теплового потока и скорости уноса капель при разрыве пузырьков в случае кипения пленок жидкости, стекающих вниз по внешней поверхности равномерно нагреваемой вертикальной трубы. Критическое условие возникает вначале на выходе из нагреваемого участка. Критический тепловой поток характеризуется тремя отличительными особенностями, которые наблюдаются по мере увеличения скорости течения жидкой пленки на выходе из нагреваемого участка. Полученные результаты выражены через скорость течения пленки и число Вебера для пленки на выходе из участка. Обсуждается соотношение между скоростью уноса капель и скоростью испарения пленки.